Development of new remote sensing methods for mapping green vegetation and exposed bedrock fractions within heterogeneous landscapes

Y.M. Yue [a] [b] , K.L. Wang [a] [b] , B. Liu [c] , R. Li [d] , B. Zhang [d] , H.S. Chen [a] [b] & M.Y. Zhang [a] [b]

[a] Key Laboratory of Agro-ecological Processes in Subtropical Region , Institute of Subtropical Agriculture, Chinese Academy of Sciences , Changsha , Hunan , 410125 , China

[b] Huanjiang Experimental Stations of Karst Ecosystem, Chinese Academy of Sciences , Huanjiang , Guangxi Province , 547100 , China

[c] Nanjing Institute of Environmental Sciences, Ministry of Environmental Protection of China , Nanjing , 210042 , China

[d] Institute of Remote Sensing and Digital Earth, Chinese Academy of Sciences , Beijing , 100094 , China
Published online: 15 Apr 2013.

PLEASE SCROLL DOWN FOR ARTICLE

of information. Taylor and Francis shall not be liable for any losses, actions, claims, proceedings, demands, costs, expenses, damages, and other liabilities whatsoever or howsoever caused arising directly or indirectly in connection with, in relation to or arising out of the use of the Content.

This article may be used for research, teaching, and private study purposes. Any substantial or systematic reproduction, redistribution, reselling, loan, sub-licensing, systematic supply, or distribution in any form to anyone is expressly forbidden. Terms & Conditions of access and use can be found at http://www.tandfonline.com/page/terms-and-conditions

Taylor & Francis
Taylor & Francis Group

Development of new remote sensing methods for mapping green vegetation and exposed bedrock fractions within heterogeneous landscapes

Y.M. Yue[a,b], K.L. Wang[a,b]*, B. Liu[c], R. Li[d], B. Zhang[d], H.S. Chen[a,b], and M.Y. Zhang[a,b]

[a]*Key Laboratory of Agro-ecological Processes in Subtropical Region, Institute of Subtropical Agriculture, Chinese Academy of Sciences, Changsha, Hunan 410125, China;* [b]*Huanjiang Experimental Stations of Karst Ecosystem, Chinese Academy of Sciences, Huanjiang, Guangxi Province 547100, China;* [c]*Nanjing Institute of Environmental Sciences, Ministry of Environmental Protection of China, Nanjing 210042, China;* [d]*Institute of Remote Sensing and Digital Earth, Chinese Academy of Sciences, Beijing 100094, China*

Karst rocky desertification is a process of land desertification associated with human disturbance of the fragile karst ecosystems. The fractional cover of photosynthetic vegetation (PV) and exposed bedrock (Rock) are the main land-surface symptoms of karst rocky desertification. In this study, we explored a new methodology for quantifying PV and Rock by remote sensing. To reduce the effects of the high heterogeneity of karst landscapes on vegetation information extraction, a whole image was segmented into relatively homogeneous subsets and then the PV was estimated using a normalized difference vegetation index spectral mixture analysis (NDVI-SMA) model. The percentage of Rock was estimated using a karst rocky desertification synthesis index (KRDSI) and lignin cellulose absorption index (LCA). The results showed that the heterogeneity of a complex landscape is a major factor in the uncertainty of PV retrievals. The fractional cover of PV can be accurately estimated by the proposed method, but might be underestimated using NDVI and overestimated using the SMA-NDVI model. The bedrock fractions can be rapidly and objectively estimated with Hyperion or simulated Advanced Spaceborne Thermal Emission and Reflection Radiometer (ASTER) imagery. Compared with multispectral images, hyperspectral images could be used to estimate PV and Rock more accurately. Our findings indicate that PV and Rock can be directly and efficiently quantified using remote sensing techniques within heterogeneous landscapes.

1. Introduction

Karst regions are typically ecologically fragile zones constrained by the local geology (Wang, Liu, and Zhang 2004; Yuan and Zhang 2008; Parise, Wales, and Gutierrez 2009). Southwest China is one of the largest karst regions in the world, covering about 540,000 km, within which more than 220,000,000 people live. Over the past few decades, this area has experienced an overwhelming rate of the so-called karst rocky desertification (KRD), a special land degradation process involving high erosion rates, extensive exposure of bedrock,

---

*Corresponding author. Email: hnyym829@163.com

drastic decreases in soil productivity, and the appearance of a desert-like landscape (Wang, Liu, and Zhang 2004). It is caused by unsustainable intensive land use on a fragile karst geo-ecological environment (Cao, Yuan, and Pei 2005). The process is expanding rapidly, and it is reducing the living space of residents. It is also the root cause of drought, water-logging, and poverty in the karst regions of southwest China. Consequently, the carrying capability of the land has declined significantly. KRD, along with sandy desertification in northwest China and soil and water loss on the Loess Plateau, is one among the most serious ecological and environmental problems in China (Chinese Academy of Sciences 2003).

Karst geomorphology developed on carbonate rocks. KRD is closely correlated to the distribution of pure carbonate rocks, with a lower percentage of acid-insoluble residue (Wang, Liu, and Zhang 2004). When KRD develops, the most obvious land-surface symptoms are the exposure of carbonate rocks and low vegetation cover. So, the fractional cover of exposed carbonate rocks and vegetation are most commonly represented as the land-surface symptoms of KRD. In addition, landscapes in karst environments include discontinuously distributed soil and fragmented ecological spaces suitable for plants. Therefore, the karst landscape has spatially high heterogeneity, rendering it difficult to accurately extract the main land-surface symptoms of KRD.

At present, research on KRD mainly depends on ground survey of the vegetation and exposed bedrock (Rock) fractions, soil erosion rates, vegetation type and structure, average soil depth, and related statistical data to classify and qualitatively assess the degree and extent of KRD. These methods are often time consuming, labour intensive, and limit multi-temporal comparison and large-scale research on KRD (Wang and Li 2007). Because of the inherent merits of remote sensing technology, some recent research has started using it to monitor and assess KRD (Huang and Cai 2007, 2009; Yue et al. 2010; Yang et al. 2011). These methods mostly first chose the appropriate indicators of KRD, then ascertain the interpretation standards of images, and finally focus on visual interpretation and computer-assisted digital processing of satellite images. Although this procedure to some extent is accurate and comprehensive, it depends on the analysts' level of experience and is of low efficiency (Huang and Cai 2009).

Fractional ground cover extracted from satellite images has been widely used to estimate land degradation and human disturbances (Hill, Megier, and Mehl 1995; Armston et al. 2009; Kim and Daigle 2011). As key ecological indicators, the fractional cover of photosynthetic vegetation (PV, green vegetation) and the percentage of Rock are widely used to characterize the main land-surface symptoms of KRD (Wang, Liu, and Zhang 2004; Wang and Li 2005). In regions of KRD, the distributions of PV, limestone soils, carbonate rocks, and non-PV (aboveground dead biomass, litter, and wood) are mixed – distributed with vegetation fragmentation and soil discontinuity. Li et al. (2009) demonstrated that the effects of grain of spatial variation on karst landscapes and the fractional cover of shrub, Rock, and bare soil would increase at higher spatial resolution, whereas the dry land and sparse woodland fractions would decrease and forest cover would fluctuate. In addition, the implementation of ecological construction projects (e.g. Karst Rocky Desertification Comprehensive Control and Restoration Project and the Grain to Green Programme) and the damage and reclamation of forest and grassland coexist, resulting in karst landscapes being in a fluctuating state of restoration and degradation (Li et al. 2005). Therefore, karst landscapes are highly heterogeneous and even relatively fine-resolution (e.g. SPOT 10 × 10 m) remote-sensing data do not record pure vegetation spectra, but rather the mixed reflectance of green vegetation, non-PV, Rock, and bare soil. This makes

it difficult to estimate the surface area of PV and Rock accurately by remote sensing (Yue et al. 2010; Zhang, Hu, and Xiao 2010).

To estimate the proportions of land cover at the sub-pixel scale, one commonly used approach is spectral mixture analysis (Pu, Gong, and Michishita 2008). However, this approach is problematic owing to spatial variation in endmember selection when used in practice, especially for highly heterogeneous landscapes in karst regions (Yue et al. 2010). Another widely used method is based on the regression of vegetation indices and fractional cover. The performance and suitability of a particular index are generally determined by the sensitivity of the index to characteristics of interest (Haboudane, Miller, and Pattey 2004). However, vegetation indices are not easily applicable to all land-cover types, especially the Rock widely distributed in karst regions. Many studies have focused on improving vegetation indices by proposing colour, form, enhanced, and intensity indices for mapping land degradation (Huete, Miura, and Gao 2003). However, these indices have mainly been used to estimate the fractional cover of PV and are not fit to extract the cover information of Rock (Yue et al. 2010, 2011). In addition, the high spatial heterogeneity of karst landscapes will also affect the accuracy of vegetation coverage estimation (Johnson and Xie 2011; Giner and Rogan 2012).

Rapid and efficient acquisition of the proportion of Rock is critical for monitoring and assessing of the degree and extent of KRD within a complex landscape (Cao, Yuan, and Pei 2005). Currently, there are few direct, objective, and efficient remote sensing methods available to assess the fractional cover of Rock by remote sensing (Huang and Cai 2009; Dunhill 2011). Huang and Cai (2009) proposed the normalized difference rock index (NDRI) to map karst rock rapidly. However, this method is limited by the differentiation of the pixel values of karst rock in built-up areas. Zhang, Hu, and Xiao (2010) suggested using the bare soil index (BI) to extract the proportion of Rock in karst regions directly. However, they failed to consider the effects of changes in vegetation phenology on fractional cover estimation. During the plant-senescent period, the fractional cover of non-PV significantly influences the estimation of the Rock area (Asner et al. 2000; Chabrilat et al. 2004; Yue et al. 2011). Therefore, it is necessary to explore new methodological approaches for estimating the fractional cover of PV and exposed bedrocks for KRD monitoring and assessment.

Rather than a new mechanistic model, we propose a simple mathematical approach that could be used to extract the land-surface symptoms of KRD directly and automatically within complex landscapes. The remote sensing method proposed could be more accurate for the mapping of green vegetation and Rock fractions in the highly heterogeneous karst landscapes of southwest China. For the estimation of PV cover, we combined an improved image segmentation step and normalized difference vegetation index (NDVI)-based model, which took the effects of background heterogeneity into consideration. For the estimation of bedrock fractions, we employed our previously proposed and available spectral indices, which could differentiate the Rock and built-up areas and consider the effects of plant phenological status.

In our previous study, we proposed a new spectral index, the KRD synthesis index (KRDSI) for hyperspectral imagery, which was developed based on unique spectral features observed in non-vegetation land-cover types (non-PV, bare soil, and Rock) and could be used to extract the fractional cover of non-vegetation (Yue et al. 2010). However, this spectral index was assessed using field-surveyed spectral data only. Further evaluation using remote sensing images for extraction of key indicators of KRD is necessary. In addition, for comparison of bedrock fractions with multispectral imagery, we tested whether the available lignin cellulose absorption index (LCA), which was specific to Advanced Spaceborne

Thermal Emission and Reflection Radiometer (ASTER) and provided a measure of the relative depths of lignin and cellulose absorption features (Daughtry, Hunt, and Mcmurtrey 2005; Gill and Phinn 2008), could be used for extraction of bedrock fractions. Hence, in the present study, we explored the methodology for estimation of key indicators of KRD directly and objectively using satellite imagery, in particular by comparing hyperspectral and multispectral imagery.

2. Data and methods

2.1. Image collection and processing

To explore a new methodology for estimating key indicators of KRD, Earth Observing 1 (EO-1) Hyperion and simulated Earth Observing System (EOS) Terra ASTER imagery were used to further validate the extraction of PV and Rock. The EO-1 Hyperion imagery was acquired on 3 March 2008, with a spatial resolution of 30 m across a swath 7.5 km wide. It covered a typical KRD area near Qibainong in Dahua County, Guangxi Province, China (Figure 1).

A total of 176 bands of Hyperion imagery were used, atmospherically corrected with Atmospheric Correction Now (ACORN), and geometrically corrected based on a 1:50,000 digital elevation model (DEM) (Goodenough et al. 2003). In addition, ASTER imagery was simulated to compare the performances of hyperspectral and multispectral imagery for extracting indicators of KRD. High-quality ASTER imagery in parallel with Hyperion acquisition was unavailable, due to the presence of more cloudy and rainy days in rugged karst regions. Therefore, the Hyperion data were convolved to the nine visible, near-infrared, and short-wave infrared (SWIR) ASTER bands using ASTER spectral response functions and spatial resolution, which were 15 m for bands 1–3 and 30 m for bands 4–9. ASTER data are the most frequently used and typical multispectral data currently available and have more bands in SWIR compared with those in other multispectral data. For

Figure 1. Landscape view of karst rocky desertification.

more direct comparison of the advantages and disadvantages of estimation of the fractional cover of vegetation and Rock with hyperspectral Hyperion and multispectral images, the simulated ASTER was used. Several studies have shown the feasibility and efficiency of this method of data simulation (Hook et al. 2001; Hulley and Hook 2009; Serbin et al. 2009).

2.2. *Image segmentation*

In the natural world, objects in complex, highly heterogeneous environments show a characteristically continuous spatial distribution. That is, the spatially heterogeneous landscape is essentially a continuous surface (Wu 1999). Temperature, water content, soil, and vegetation have this characteristic continuity, rather than changing dramatically within a given space. This phenomenon is called 'spatial continuity' or 'spatial autocorrelation' (Koenig 1999; Fried 2000). The hypothesis of spatial autocorrelation is that objects/measurements separated by short distances are likely to be more alike than objects/measurements separated by large distances. Consequently, although there is high heterogeneity in a large-scale landscape, there may be relatively low heterogeneity in a local-scale landscape. Therefore, if we segment the images into relatively homogeneous subsets, this may reduce the effects of the high heterogeneity of the karst landscape on information extraction.

Image segmentation aims to segment the whole-scene image into spatially continuous, disjunctive, and relatively homogeneous subsets (Pekkarinen 2002). It may be one of the alternative means to suppress the effects of heterogeneity on remote sensing information extraction. Therefore, to reduce the effects of heterogeneous landscapes on vegetation coverage information extraction, the whole-scene image should be segmented into relatively homogeneous subsets. Our improved image segmentation method aims at maximizing intrasegment homogeneity and intersegment heterogeneity of the heterogeneous landscape (Martha et al. 2011). It has two main components: intrasegment metrics and intersegment disparity metrics.

For Hyperion hyperspectral imagery, intrasegment uniformity metrics were calculated with the spectral similarity of pixels in each segment. Spectral similarity is defined by the spectral angle θ. The general angle can be described by the arc cosine (Kruse, Lefkoff, and Boardman 1993):

$$\theta = \arccos \frac{T \bullet R}{|T\,\|R\,|}, \tag{1}$$

namely,

$$\theta = \arccos \frac{\sum\limits_{i=1}^{n} t_i r_i}{\sqrt{\sum\limits_{i=1}^{n} t_i^2} \sqrt{\sum\limits_{i=1}^{n} r_i^2}}, \tag{2}$$

where T and R are spectral vectors with reflectance components from two spectral bands t and r of the adjacent pixels, n is the number of spectral bands, i is the number of pixels, and θ is the general angle between T and R. The similarity of T and R increases as θ decreases. Mixed pixels having spectral similarity can be classified into the same segments. The spectral threshold is ascertained by intersegment disparity metrics.

To assess intersegment disparity, Moran's *I* autocorrelation index is used. Moran's *I* is a spatial autocorrelation metric that measures how similar a region is to its neighbours on average (Fotheringham, Brunsdon, and Charlton 2000). We chose to use Moran's *I* because it is a reliable indicator of statistical separation between spatial objects and was found to be a good indicator of segmentation quality in previous segmentation evaluation studies (Johnson and Xie 2011). For each segment, the algorithm calculates its mean spectral reflectance value and determines all adjacent segments. Moran's *I* is calculated as follows:

$$I = \frac{n \sum_{i=1}^{n} \sum_{j=1}^{n} w_{ij}(y_i - \bar{y})(y_j - \bar{y})}{\sum_{i=1}^{n} (y_i - \bar{y})^2 \left(\sum_{i \neq j} \sum w_{ij}\right)}, \tag{3}$$

where *n* is the total number of segments, w_{ij} is a measure of the spatial proximity, and y_i is the mean spectral reflectance value of the segment and is the mean spectral value of the whole image. Each weight w_{ij} is a measure of the spatial adjacency of the segments. Low Moran's *I* values indicate high intersegment heterogeneity, which is desirable for image segmentation. Therefore, our improved image segmentation method combines the low-intersegment Moran's *I* index (adjacent segments are dissimilar) with low spectral differences (each segment is relatively homogeneous).

For ASTER multispectral imagery, the spectral angle approach and Moran's *I* is not adopted for image segmentation because there are fewer bands available for ASTER imagery and the spectral differences of segments are not significantly different. Thus, it is difficult to segment ASTER based on spectral features. Instead, the whole ASTER imagery was segmented into subsets with the same size of pixel window (3×3, 5×5, 7×7 . . . or 35×35) to obtain relatively homogeneous cells based on the concept of spatial autocorrelation. Fractional cover of PV derived from the NDVI model was then compared with the real value based on fieldwork to confirm the optimal size of subsets, namely the scale of relatively homogeneous cells.

Our experimental tests showed that the field survey fractional cover was closely related to that predicted by image subsets, with pixel size 35×35, which is appropriate for ASTER segmentation. Note that we identified relatively homogeneous areas of several to many pixels potentially containing several land-cover types. However, the characteristics of adjacent 35×35-pixel segments identified may be not highly heterogeneous, and their size could be relatively similar to that of whole-image pixels due to spatial autocorrelation. This is not in conflict with the difficulty involved in capturing land-surface type even with 10×10 m SPOT imagery, which means that even at that resolution, there would be mixed ground cover in karst regions. We thus segmented images into subsets of this size, which were considered as relatively homogeneous cells, and then all processes and models were applied to these cells.

2.3. Estimation of PV with NDVI-SMA model

The fractional cover of PV of whole-scene Hyperion or ASTER images could be calculated from the per-abundance sum of each relatively homogeneous subset. The abundance of each subset of image $I_k(k = 1, \ldots, n)$ was estimated using the normalized difference vegetation index spectral mixture analysis (NDVI-SMA) model, which assumed that the NDVI value of a given pixel is a linear combination of NDVI values of PV and non-PV,

weighted by their relative proportions (Qi et al. 2000; Liu et al. 2009). If the fractional cover of green vegetation is f_{veg}, the fractional cover of non-vegetation should be $1 - f_{veg}$. Therefore, the resulting signal $S_k(i,j)$ as observed by a remote sensor can be expressed as

$$S_k(i, j) = f_{veg}(i, j) \times S_{k,veg} + (1 - f_{veg}(i, j)) \times S_{k,non\text{-}veg}, \qquad (4)$$

where $S_k(i, j)$ is the signal of each subset I_k, $S_{k,veg}$ is the signal contribution from the green vegetation component, and $S_{k,non\text{-}veg}$ is the contribution from the non-vegetation component. In addition, Equation (4) can also be applied to remotely-sensed images in the spectral vegetation index domain (Leprieur, Verstraete, and Pinty 1994). When applied with a spectral vegetation index, such as the NDVI, Equation (4) may be approximated as

$$NDVI_k(i, j) = f_{veg}(i, j) \times NDVI_{k,veg} + (1 - f_{veg}(i, j)) \times NDVI_{k,non\text{-}veg}, \qquad (5)$$

which can be rewritten as

$$f_{veg}(i, j) = \frac{NDVI_k(i, j) - NDVI_{k,non\text{-}veg}}{NDVI_{k,veg} - NDVI_{k,non\text{-}veg}}, \qquad (6)$$

where $NDVI_{k,veg}$ is the *NDVI* value of a vegetation pixel and $NDVI_{k,non\text{-}veg}$ is the value of an area of non-vegetation in I_k.

The main problem when applying Equation (6) is the correct identification of $NDVI_{k,veg}$ and $NDVI_{k,non\text{-}veg}$. There have been two main approaches proposed to retrieve $NDVI_{k,veg}$ and $NDVI_{k,non\text{-}veg}$ values based on image statistics (Jimenez-Munoz et al. 2009). The first retrieves them from the NDVI histogram, which requires sufficient bare non-vegetation and fully vegetated pixels in the image. Hence, it is not suitable for highly heterogeneous karst environments. The second approach chooses the maximum and minimum NDVI values for the whole scene as the $NDVI_{k,veg}$ and $NDVI_{k,non\text{-}veg}$ values. This approach assumes that pixels with $f_{veg(i,j)} = 0$ and $f_{veg(i,j)} = 1$ exist throughout the image. We used this approach, choosing the maximum and minimum NDVI values for each subset of I_k as $NDVI_{k,veg}$ and $NDVI_{k,non\text{-}veg}$. The minimum and maximum NDVI values, and their variations within the studied data subsets of Hyperion and simulated ASTER, are shown in Table 1. Compared with the mean values of $NDVI_{max}$ and $NDVI_{min}$ suggested by Jiménez-Muñoz et al. (2009; respectively 0.9 and 0.15), the $NDVI_{min}$ and $NDVI_{max}$ selected were relatively smaller. This may due to the effects of terrain shadows on karst landscapes.

In addition, NDVI values obtained from ground spectral measurements of each component (Rock, green vegetation, non-PV, and bare soil) and of their variations were conducted simultaneously with the *in situ* measurements of fractional cover (Table 2). Compared with the NDVI values obtained from ground measurements of each component, the selected local minimum and maximum values at image subset level were reasonable for their similar threshold values.

Table 1. Minimum and maximum NDVI values and their variations within the data subsets of Hyperion and simulated ASTER studied.

	NDVI$_{max}$	NDVI$_{min}$
Hyperion$_{subsets}$	0.73 ± 0.26	0.25 ± 0.14
ASTER$_{subsets}$	0.67 ± 0.21	0.19 ± 0.11

Table 2.   Mean NDVI values obtained from ground measurements of each component and their variations.

	PV	Non-PV	Soil	Rock
$NDVI_{in\text{-}situ}$	0.84 ± 0.06	0.35 ± 0.11	0.17 ± 0.05	0.29 ± 0.13

To compare the estimation of the proportion of vegetation under highly heterogeneous karst ecosystems to that of the proposed method, the NDVI and NDVI-SMA models were also employed.

2.4.   *Strategies for extracting the proportion of Rock with Hyperion and ASTER*

Two major methodological approaches for extracting the area of Rock in an image have been proposed using hyperspectral and multispectral imagery. To extract key indicators of KRD from hyperspectral images, our previously proposed KRDSI, which was used to characterize and accentuate the spectral absorption features of bedrock using the short-wave infrared (SWIR 2000–2400 nm) wavelengths, could directly be used to extract the proportion of exposed rock from images (Yue et al. 2010):

$$KRDSI = \rho_0 - \rho_c, \tag{7}$$

where ρ is the pixel spectral reflectance in the SWIR; a, b, and c are the wavelengths of the two shoulders and the peak absorption features of carbonate rocks in SWIR, which appear as an absorption feature centred at 2350 nm; and ρ_0 is the estimated reflectance at wavelength c, assuming there were no absorption features present and therefore interpolating linearly between reflectances at wavelengths a and b (Yue et al. 2010).

To extract Rock fractions with multispectral imagery, we employed LCA, which was previously shown to be linearly related to the fractional cover of bare ground and crop residue (Daughtry, Hunt, and Mcmurtrey 2005; Gill and Phinn 2008):

$$LCA = 100 \times [(ASTER\,6 - ASTER\,5) + (ASTER\,6 - ASTER\,8)], \tag{8}$$

where ASTER5, ASTER6, and ASTER8 are the spectral reflectance of ASTER bands 5 (2.145–2.185 µm), 6 (2.185–2.225 µm), and 8 (2.295–2.365 µm) in SWIR, respectively. Our ground measurements of LCA and the proportion of non-PV and bare soil showed that LCA was linearly related to the proportion of non-PV and bare soil ($p < 0.05$, Figure 2). Consequently, the fractional cover of non-PV and soil could be assessed with LCA and ASTER. As the main land-cover types of KRD are PV, non-PV, Rock, and bare soil, Rock could be estimated by subtracting the fractional cover of PV, soil, and non-PV.

2.5.   *Validation of extraction of PV and Rock with Hyperion and ASTER*

The validation experiment was carried out between 28 March and 7 April 2009. We used field survey data to validate the accuracy of the extraction of indicators for evaluating KRD with Hyperion and simulated ASTER. The ground points were selected using the stratified random-sampling method. The fractional cover of vegetation was stratified as 0–20%, 20–40%, 40–60%, 60–80%, and more than 80%, while Rock was 0–15%, 15–30%, and
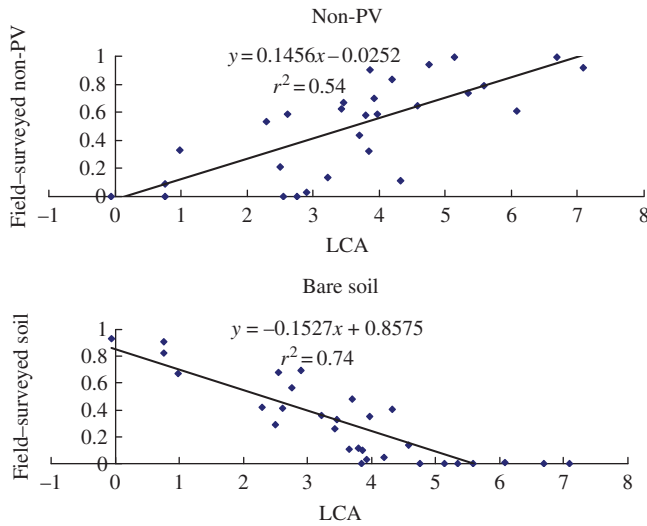
Figure 2. The linear relationship between field-surveyed proportion of non-PV, bare soil, and LCA.

30–50%. A total of 36 plots were selected, the sample size of each being 90 × 90 m. Because mixed phenomena were severe for the highly heterogeneous karst environments and poor accessibility in rugged karst regions, only 21 effective plots were ultimately used. The main types of vegetation cover were shrub and open shrublands. Visual observations, photography, and transect sampling methods were combined to estimate the fractional cover of PV and Rock in each plot (Zhou, Robson, and Pilesjo 1998; Delameter et al. 2012). For the transect sampling method, two 90 m measuring tapes are laid in a cross-shape (Figure 3). The first is orientated north to south and the second at 90° to north. An observation of ground cover (green vegetation, non-PV, Rock, and bare soil) is made for every 1 m, starting at the 1 m point of each transect.

The remotely-sensed coverage of each pixel was averaged with its neighbourhood pixels (3 × 3 pixel window) and extracted from the coverage images according to its location determined by a global positioning system (GPS). The results of validation are represented by the coefficient of determination R^2 and cross-validation RMSE of the linear relationship between field survey fractional cover and that predicted by Hyperion and ASTER.
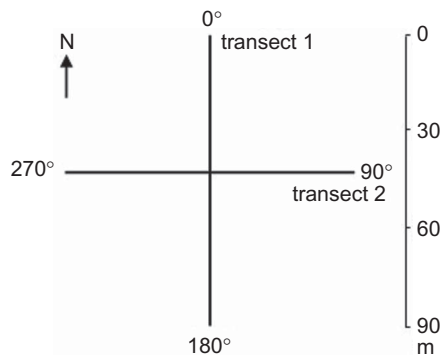

Figure 3. The two transects lying in each plot.

3. Results

3.1. *Reducing the effects of high heterogeneity of karst landscape on PV estimation*

Hyperion hyperspectral imagery was segmented to reduce the effects of heterogeneity with the combination of spectral similarity of pixels and Moran's *I* index of adjacent segments. Figure 4(*a*) shows how Moran's *I* index varies with varying spectral angle threshold. In a comparison of spectral similarity threshold with spectral angles of 5°, 7.5°, and 10° (Figure 4(*b*)), segmentation with the spectral angle threshold of 7.5° achieved the lowest value of Moran's *I* (0.047), which indicates low spatial autocorrelation. Every segment is internally homogeneous and is dissimilar to its adjacent segments. Due to highly heterogeneous environments, it is likely that spectral similarity will continue to decrease as segmentation scale increases, and Moran's *I* will continue to decrease until segments become sufficiently large to contain a mixture of different types of land cover (Espindola et al. 2006; Johnson and Xie 2011).

PV predicted by the NDVI-SMA model, with relatively homogeneous subsets of Hyperion, was the closest to field-surveyed PV, while that predicted by either the NDVI or NDVI-SMA models without pre-segmentation of the whole Hyperion image was inferior (Figure 5), being underestimated by NDVI and overestimated by NDVI-SMA.

For ASTER multispectral imagery, we segmented the whole image into relatively homogeneous subsets at a size of 35×35 pixels, to reduce the high heterogeneity within the whole image. Estimation of PV with the pre-segmented ASTER image was less accurate than that using Hyperion. However, results derived from the pre-segmented image were far superior to those derived from the image without pre-segmentation (Figure 6).
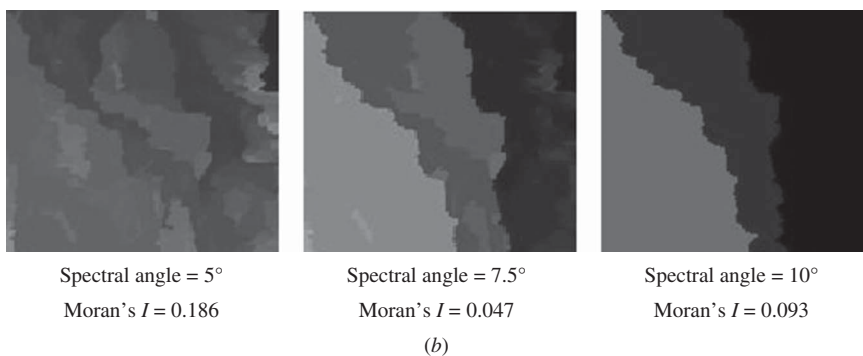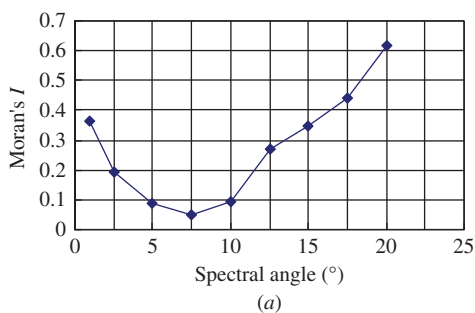

(*a*)

| Spectral angle = 5° | Spectral angle = 7.5° | Spectral angle = 10° |
| Moran's *I* = 0.186 | Moran's *I* = 0.047 | Moran's *I* = 0.093 |

(*b*)

Figure 4. (*a*) Moran's *I* index varies with different spectral angle threshold. (*b*) Image segmentation with different spectral similarity threshold.
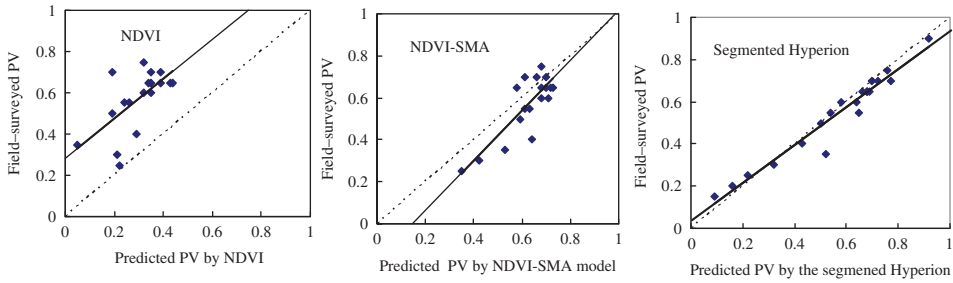
Figure 5.   Scatter diagram with a 1:1 straight line (dashed line) and fitting line (solid line) of PV predicted by Hyperion using field-surveyed, NDVI, NDVI-SMA model, and NDVI-SMA with segmented Hyperion.
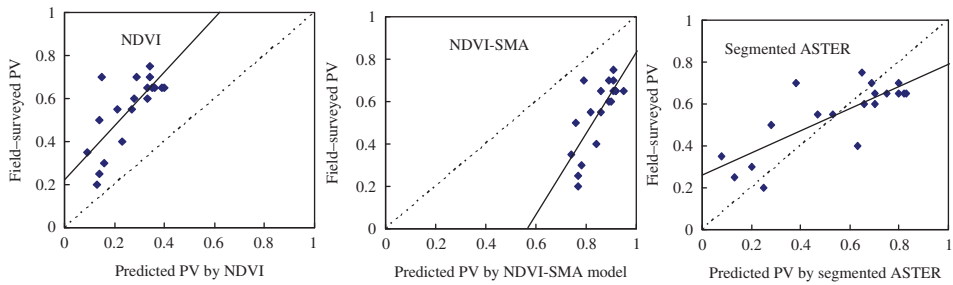

Figure 6.   Scatter diagram with a 1:1 straight line (dashed line) and fitting line (solid line) of PV predicted by ASTER using field-surveyed, NDVI, NDVI-SMA model, and NDVI-SMA with segmented ASTER.

It also underestimated PV when using NDVI and overestimated it when using NDVI-SMA. When comparing the NDVI and NDVI-SMA models, the proposed method with Hyperion hyperspectral imagery and ASTER multispectral imagery supported our hypothesis that segmentation of the whole image into relatively homogeneous subsets will reduce the effects of high landscape heterogeneity on the extraction of vegetation information.

3.2.   *Estimation of PV and ock with EO-1 Hyperion*

The linear regression of predicted fractional cover of PV and Rock is shown in Figure 7. The PV estimated with Hyperion after pre-segmentation, as described above, closely correlated with field-surveyed PV, and the coefficient of determination R^2 was 0.95. The results of using KRDSI to assess Rock were less accurate, with R^2 of 0.53. This might have been due to the fact that the proposed KRDSI did not consider the effects of weathering processes on exposed bedrocks, which would result in variability in the absorption features of carbonate rocks, thus affecting the absorption features captured and characterized by KRDSI (Younis et al. 1997; Yue et al. 2010).

3.3.   *Estimation of PV and Rock with ASTER*

As the LCA was linearly related to the fractional cover of soil and non-PV, it was employed to extract the fractional cover of Rock. Accordingly, this was estimated by subtracting the
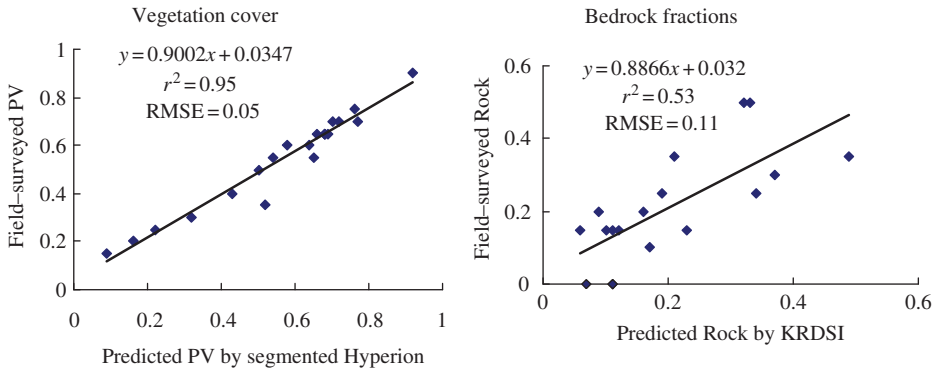
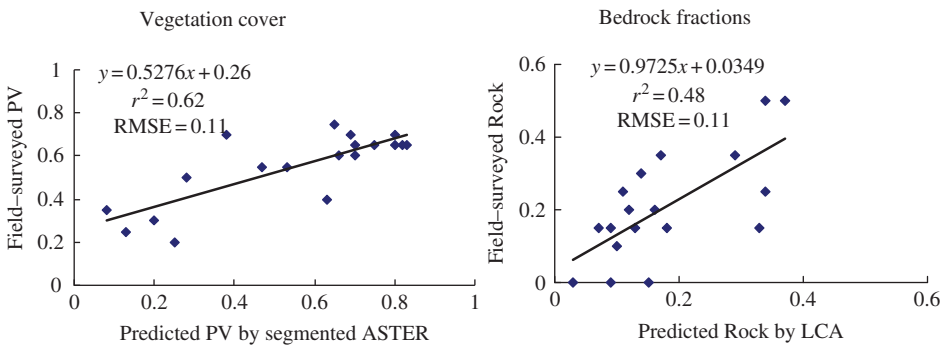Figure 7.   PV and Rock predicted by EO-1 Hyperion.

Figure 8.   PV and Rock predicted by simulated ASTER.

fractional cover of vegetation, soil, and non-PV. There was a significantly positive correlation between field-surveyed PV and that predicted by ASTER imagery (Spearman: $R^2 = 0.79$, $p = 0.00006$), as well as between field-surveyed Rock and that predicted by ASTER imagery (Spearman: $R^2 = 0.69$, $p = 0.001$). The linear regressions of field-surveyed cover and those predicated by ASTER showed that PV and Rock could be directly estimated with multispectral imagery (Figure 8). However, the results were not as accurate as those of Hyperion, mainly due to the limits of multispectral bands, which cannot identify spectral differences between ground objects in the highly heterogeneous karst ecosystems.

3.4.   Comparison of hyperspectral and multispectral imagery for estimating the land-surface symptoms of KRD

The spatial distributions of PV and Rock as estimated by Hyperion and ASTER are shown in Figure 9. As indicated in the figure, higher PV leads to lower Rock. Note that we did not take the vegetation cover types and structure into consideration here. Thus, the fractional cover of green vegetation and Rock reveals the main land-surface symptoms of KRD clearly. Compared with ASTER multispectral imagery, Hyperion hyperspectral imagery estimated the fractional cover of PV and Rock more efficiently.
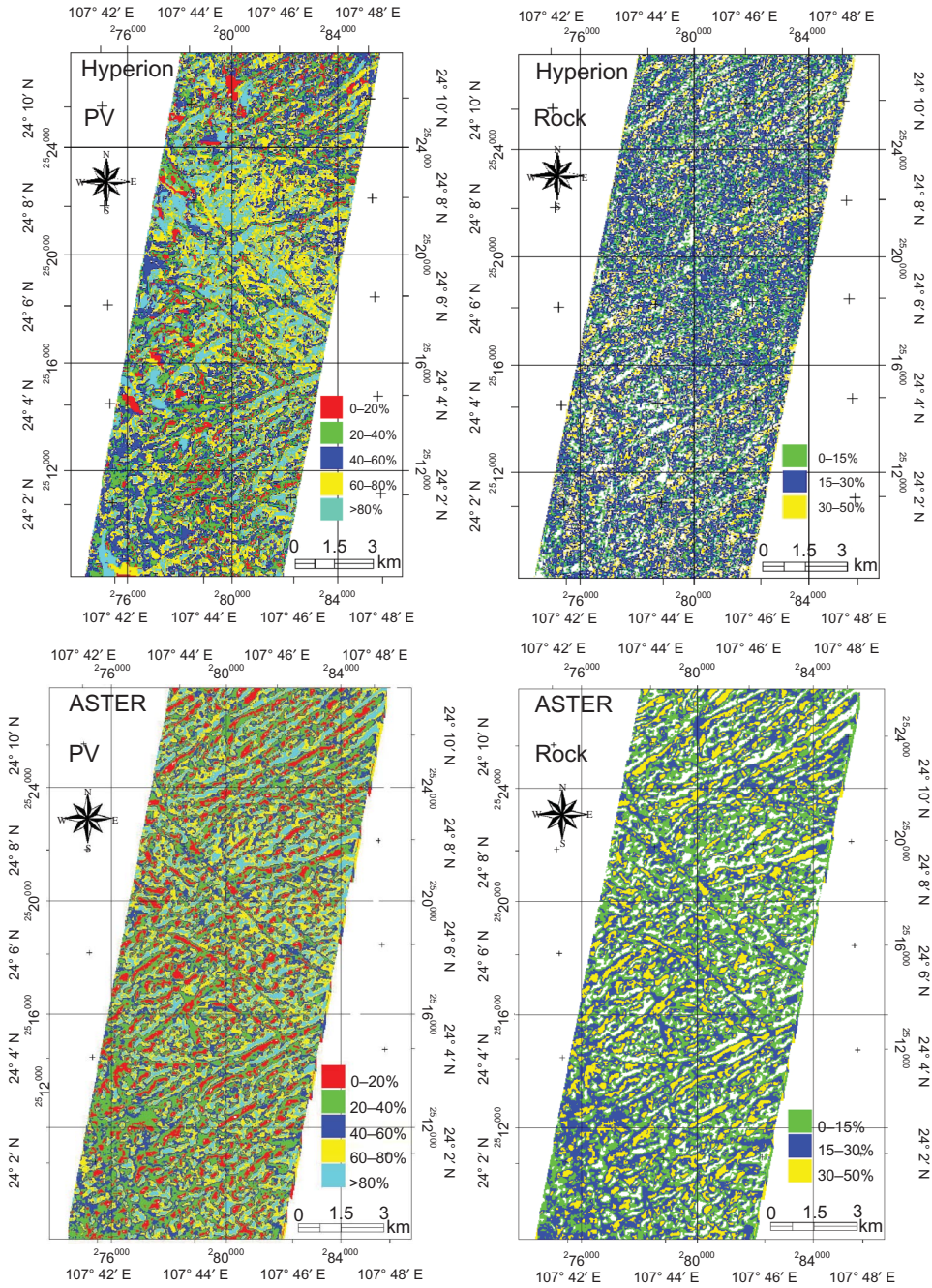
Figure 9.   Mapping of PV and Rock with Hyperion and simulated ASTER imagery.

4.   Discussion

The literature on remote sensing of KRD has paid scant attention to the mixed distribution of ground objects in karst landscapes and has not taken into consideration the effects of high heterogeneity on remote sensing information extraction (Huang and Cai 2009; Zhang, Hu,

and Xiao 2010). Our study examined the potential of using remote sensing technology for direct and objective estimation and mapping of PV and Rock in heterogeneous landscapes. This will be of potential use in quantifying the main land-surface symptoms of KRD.

Compared with traditional remote sensing methods, our suggested method can be used to estimate vegetation fractional cover more accurately and demonstrates that considerable spatial heterogeneity may underlie accurate PV measurements. Jiang, Zhang, and Sun (2011) showed that the heterogeneity within a pixel might lead to scale effects for water–land boundaries in the retrieval of PV. Johnson and Xie (2011) also suggested taking into account the heterogeneity traits when identifying optimal image segmentation. Giner and Rogan (2012) indicated that Landsat ETM+ imagery was adequate for mapping the fractional cover of larger, contiguous patches of forest, but its spatial resolution was too coarse for accurate mapping of highly fragmented, spatially complex landscapes. Therefore, the heterogeneity of a complex landscape is a major reason for uncertainty in the retrieval of vegetation coverage. It is possible and necessary to segment images of considerable spatial heterogeneity into relatively homogeneous subsets. Although the non-linear sub-pixel method might be effective in estimating the fractional cover of vegetation under complex landscapes, calculations are complex (Liu and Wu 2005; Jiapaer, Chen, and Bao 2011). Use of this method is also likely to be problematic for other areas similar to karst regions with a mixed distribution of ground objects and high heterogeneity.

Although our proposed method for bedrock fractions was not as accurate as the prediction of PV, it makes the task of rapidly and automatically quantifying bedrock fractions less laborious and more accurate with remote sensing images on the larger scale. The main limitation of the estimation of bedrock fractions with Hyperion hyperspectral imagery is the fact that KRDSI does not consider the effects of weathering processes on carbonate rocks and the spectral differences between dolomite and limestone, whose absorption features were centred at 2300 and 2340 nm, respectively (Fu 1996; Yue et al. 2010). The outcome of using simulated ASTER multispectral imagery was influenced by the error accumulation of the fractional cover of bare soil and non-PV estimation with LCA, which was designed to estimate crop residue cover (Daughtry, Hunt, and Mcmurtrey 2005; Serbin et al. 2009). In addition, the shadow effects of terrain-related problems, which would induce variation in slope/aspect, illumination, and shading, may also cause uncertainty in the estimation of bedrock fractions. In future studies, the spectral features of Rock and improvements in LCA would be needed to obtain a more accurate estimation of bedrock fractions.

Compared with simulated ASTER multispectral imagery, Hyperion hyperspectral imagery more accurately estimated PV and Rock. The fractions predicted by Hyperion were closely correlated with field-surveyed fractional cover, with a higher R^2, and lower RMSE. In addition, those areas with a PV cover of more than 60% were accurately extracted by Hyperion but were underestimated by ASTER (Figures 6, 9). It was due to the fact that Hyperion had more bands and higher spectral resolution than ASTER in SWIR that it was possible to distinguish spectral features among non-PV, bare soil, and Rock. Hyperspectral imagery is suitable for regional KRD surveys, but may be inappropriate on a larger scale due to limitations of coverage width and the availability of hyperspectral imagery. Our method may not have fully utilized Hyperion data (Goetz 2009), but still achieved good performance in estimating the fractional cover of vegetation and exposed bedrocks. In future, our method needs further improvement before imaging spectroscopy can be recommended for KRD research.

The validation method in this study was mainly focused on the statistical scatter plots of field-surveyed and remotely-sensed coverage data. Because of the low number of ground-truth plots, we should be cautious about directly applying a statistical model

built from field-surveyed data. In addition, fractional coverage can be measured by the optical imaging method for relatively homogeneous regions using high-resolution spatial images. However, in rugged karst areas, examining remotely-sensed images based on field-surveyed methods may increase uncertainty due to severe mixed-pixel problems and sample size (Curran and Williamson 1986; Stehman et al. 2003). Therefore, our proposed method appears to be reasonably reliable for quantifying green vegetation and Rock fractions in karst regions.

Note that due to the complexity of the development and driving forces of KRD (Cao, Yuan, and Pei 2005), the mapping of green vegetation and Rock fractions should not translate directly to mapping of the degree and classification of KRD, which should consider additional information such as soil erosion rates, vegetation types and structure, average soil depth, and driving forces (Wang and Li 2005). The main drawback of this study is that simultaneous acquisition of high-quality ASTER and Hyperion images was not possible due to the number of cloudy and rainy days in rugged karst regions. When this hurdle is overcome, our methods for extraction of land-surface symptoms of KRD can be applied more effectively and accurately.

5. Conclusions

This study suggests that fractional cover of vegetation and Rock can be quantified directly and objectively with Hyperion hyperspectral and simulated ASTER multispectral imagery within a complex landscape. The high heterogeneity of karst ecosystems is a major reason for uncertainty in the retrieval of vegetation coverage. However, segmentation of the whole image into relatively homogeneous subsets can reduce its effects. The fractional cover of vegetation can be accurately estimated by combining pre-segment processing and an NDVI-SMA model, but may be underestimated with NDVI and overestimated with the NDVI-SMA model. Rock fractions can be rapidly and efficiently estimated with Hyperion hyperspectral imagery and KRDSI, or with ASTER multispectral imagery and LCA. Compared with a multispectral image, a hyperspectral image can be used to estimate the fractional cover of vegetation and Rock more accurately across a complex landscape.

Acknowledgements

References

Armston, J. D., R. J. Denham, T. J. Danaher, P. F. Scarth, and T. N. Moffiet. 2009. "Prediction and Validation of Foliage Projective Cover from Landsat-5 TM and Landsat-7 ETM+ Imagery." *Journal of Applied Remote Sensing* 3: 033540.
Asner, G. P., C. A. Wessman, C. A. Bateson, and J. L. Privette. 2000. "Impact of Tissue, Canopy and Landscape Factors on Reflectance Variability of Arid Ecosystems." *Remote Sensing of Environment* 74: 69–84.
Cao, J. H., D. X. Yuan, and J. G. Pei. 2005. *Karst Ecosystem of Southwest China Constrained by Geological Setting*. Beijing: Geological Press.

Chabrilat, S., H. Kaufmann, A. Palacios-Oryeta, P. Escribano, and A. Mueller. 2004. "Development of Land Degradation Spectral Indices in a Semiarid Mediterranean Ecosystem." *Proceedings of SPIE* 5574: 235–243.

Chinese Academy of Sciences. 2003. "Several Suggestions for the Comprehensive Taming to Karst Mountain Areas in Southwest China." *Bulletin Chinese Academy of Sciences* 3: 169.

Curran, P. J., and H. D. Williamson. 1986. "Sample Size for Ground and Remotely Sensed Data." *Remote Sensing of Environment* 20: 31–41.

Daughtry, C. S. T., E. R. Hunt Jr., and P. C. Mcmurtrey. 2005. "Remote Sensing the Spatial Distribution of Crop Residues." *Agronomy Journal* 97: 864–871.

Delameter, P. L., J. P. Messina, J. G. Qi, and M. A. Cochrane. 2012. "A Hybrid Visual Estimation Method for the Collection of Ground Truth Fractional Coverage Data in a Humid Tropical Environment." *International Journal of Applied Earth Observation and Geoinformation* 18: 504–514.

Dunhill, A. M. 2011. "Using Remote Sensing and a Geographic Information System to Quantify Rock Exposure Area in England and Wales: Implications for Paleodiversity Studies." *Geology* 39: 111–114.

Espindola, G. M., G. Camara, I. A. Reis, L. S. Bins, and A. M. Monteiro. 2006. "Parameter Selection for Region-Growing Image Segmentation Algorithms Using Spatial Autocorrelation." *International Journal of Remote Sensing* 27: 3035–3040.

Fotheringham, A., C. Brunsdon, and M. Charlton. 2000. *Quantitative Geography: Perspectives on Spatial Analysis*. Thousand Oaks, CA: Sage.

Fried, M. 2000. "Continuities and Discontinuities of Place." *Journal of Environmental Psychology* 20: 193–205.

Fu, B. H. 1996. "A Study on Reflectance Spectra Features of Carbonate Rocks and Its Application." *Rock and Mineral Analysis* 15: 207–209.

Gill, T. K., and S. R. Phinn. 2008. "Estimates of Bare Ground and Vegetation Cover from Advanced Spaceborne Thermal Emission and Reflection Radiometer (ASTER) Short-Wave-Infrared Reflectance Imagery." *Journal of Applied Remote Sensing* 2: 023511.

Giner, N. M., and J. Rogan. 2012. "A Comparison of Landsat ETM+ and High-Resolution Aerial Orthophotos to Map Urban/Suburban Forest Cover in Massachusetts, USA." *Remote Sensing Letters* 3: 667–676.

Goetz, A. F. H. 2009. "Three Decades of Hyperspectral Remote Sensing of the Earth: A Personal View." *Remote Sensing of Environment* 113: s5–s16.

Goodenough, D. G., A. Dyk, K. O. Niemann, I. S. Pearlman, H. Chen, T. Han, M. Murdoch, and C. West. 2003. "Processing Hyperion and ALI for Forest Classification." *IEEE Transactions on Geoscience and Remote Sensing* 41: 1321–1331.

Haboudane, D., J. R. Miller, and E. Pattey. 2004. "Hyperspectral Vegetation Indices and Novel Algorithms for Predicting Green LAI of Crop Canopies: Modeling and Validation in the Context of Precision Agriculture." *Remote Sensing of Environment* 90: 337–352.

Hill, J., J. Megier, and W. Mehl. 1995. "Land Degradation, Soil Erosion and Desertification Monitoring in Mediterranean Ecosystems." *Remote Sensing of Environment* 12: 237–260.

Hook, S. J., J. J. Myers, K. J. Thome, M. Fitzgerald, and A. B. Kahle. 2001. "The MODIS/ASTER Airborne Simulator (MASTER)-a New Instrument for Earth Science Studies." *Remote Sensing of Environment* 76: 93–102.

Huang, Q. H., and Y. L. Cai. 2007. "Spatial Pattern of Karst Rock Desertification in the Middle of Guizhou Province, Southwestern China." *Environmental Geology* 52: 1325–1330.

Huang, Q. H., and Y. L. Cai. 2009. "Mapping Karst Rock in Southwest China." *Mountain Research and Development* 29: 14–20.

Huete, A. R., T. Miura, and X. Gao. 2003. "Land Cover Conversion and Degradation Analyses Through Coupled Soil-Plant Biophysical Parameters Derived From Hyperspectral EO-1 Hyperion." *IEEE Transactions on Geoscience and Remote Sensing* 41: 1268–1276.

Hulley, G. C., and S. J. Hook. 2009. "Intercomparison of Versions 4, 4.1 and 5 of the MODIS Land Surface Temperature and Emissivity Products and Validation with Laboratory Measurements of Sand Samples Form the Namib Desert, Namibia." *Remote Sensing of Environment* 113: 1313–1318.

Jiang, M., X. F. Zhang, and Q. Sun. 2011. "Vegetation Coverage Retrieval Scale Effect Analysis Using Multi-Sensor Data." *Geomatics and Information Science of Wuhan University* 36: 311–315.

Jiapaer, G. L., X. Chen, and A. M. Bao. 2011. "A Comparison of Methods for Estimating Fractional Vegetation Cover in Arid Regions." *Agricultural and Forest Meteorology* 151: 1698–1710.

Jimenez-Munoz, J. C., J. A. Sobrino, A. Plaza, L. Guanter, J. Moreno, and P. Martinez. 2009. "Comparison Between Fractional Vegetation Cover Retrievals from Vegetation Indices and Spectral Mixture Analysis: Case Study of PROBA/CHRIS Data over an Agricultural Area." *Sensors* 9: 768–793.

Johnson, B., and Z. X. Xie. 2011. "Unsupervised Image Segmentation Evaluation and Refinement Using a Multi-Scale Approach." *ISPRS Journal of Photogrammetry and Remote Sensing* 66: 473–483.

Kim, M. K., and J. J. Daigle. 2011. "Detecting Vegetation Cover Change on the Summit of Cadillac Mountain Using Multi-Temporal Remote Sensing Datasets: 1979, 2001, and 2007." *Environmental Monitoring and Assessment* 180: 63–75.

Koenig, W. D. 1999. "Spatial Autocorrelation of Ecological Phenomena." *Trends in Ecology and Evolution* 14: 22–26.

Kruse, F. A., A. B. Lefkoff, and J. W. Boardman. 1993. "The Spectral Image Processing System (SIPS)-Interactive Visualization and Analysis of Imaging Spectrometer Data." *Remote Sensing of Environment* 44: 145–163.

Leprieur, C., M. M. Verstraete, and B. Pinty. 1994. "Evaluation of the Performance of Various Vegetation Indices to Retrieve Vegetation Cover from AVHRR Data." *Remote Sensing Review* 10: 265–284.

Li, Y. B., S. J. Wang, R. L. Li, and Q. Tan. 2005. "Landscape Pattern Change of Mountain-Hill Areas and Its Ecological Effects in the East of Guizhou Province." *Journal of Mountain Science* 23: 89–95.

Li, Y. B., S. J. Wang, M. W. Zhou, R. B. Li, and W. H. Li. 2009. "Spatial Resolution Effects for Landscape Patterns in the Wangjiazhai Karst Catchment." *Earth and Environment* 37: 86–90.

Liu, L. Y., J. Xia, J. H. Wang, and C. J. Zhao. 2009. "Analysis of the Changes of Vegetation Coverage of Western Beijing Mountainous Areas Using Remote Sensing and GIS." *Environmental Monitoring and Assessment* 153: 339–349.

Liu, W. G., and E. Y. Wu. 2005. "Comparison of Non-Linear Mixture Models: Sub-Pixel Classification." *Remote Sensing of Environment* 94: 145–154.

Martha, T. R., N. Kerle, C. J. Van Westren, V. Jetten, and K. V. Kumar. 2011. "Segment Optimization and Data-Driven Thresholding for Knowledge-Based Landslide Detection by Object-Based Image Analysis." *IEEE Transactions on Geoscience and Remote Sensing* 49: 4928–4943.

Parise, M., J. D. Wales, and F. Gutierrez. 2009. "Current Perspectives on the Environmental Impacts and Hazards in Karst." *Environmental Geology* 58: 235–237.

Pekkarinen, A. 2002. "A Method for the Segmentation of Very High Spatial Resolution Images of Forested Landscapes." *International Journal of Remote Sensing* 23: 2817–2836.

Pu, R. L., P. Gong, and R. Michishita. 2008. "Spectral Mixture Analysis for Mapping Abundance of Urban Surface Components from the Terra/ASTER Data." *Remote Sensing of Environment* 112: 939–954.

Qi, J., R. C. Marsett, M. S. Moran, D. C. Goodrich, P. Heilman, Y. H. Kerr, G. Dedieu, A. Chehbouni, and X. X. Zhang. 2000. "Spatial and Temporal Dynamics of Vegetation in the San Pedro River Basin Area." *Agricultural and Forest Meteorology* 105: 55–68.

Serbin, G., E. R. HuntJr, C. S. T. Daughtry, G. W. Mccarty, and P. C. Doraiswamy. 2009. "An Improved ASTER Index for Remote Sensing of Crop Residue." *Remote Sensing* 1: 971–991.

Stehman, S. V., J. D. Wickham, J. H. Smith, and L. Yang. 2003. "Thematic Accuracy of the 1992 National Land-Cover Data for the Eastern United States: Statistical Methodology and Regional Results." *Remote Sensing of Environment* 86: 500–516.

Wang, S. J., and Y. B. Li. 2005. "Discussion on the Classification of Karst Rocky Desertification in Ecological Constructions." *Carsologica Sinca* 24: 192–195.

Wang, S. J., and Y. B. Li. 2007. "Problems and Development Trends About Researches on Karst Rocky Desertification." *Advance in Earth Sciences* 6: 573–582.

Wang, S. J., Q. M. Liu, and D. F. Zhang. 2004. "Karst Rocky Desertification in Southwestern China: Geomorphology, Landuse, Impact and Rehabilitation." *Land Degradation and Development* 15: 115–121.

Wu, J. G. 1999. "Hierarchy and Scaling: Extrapolating Information Along a Scaling Ladder." *Canadian Journal of Remote Sensing* 25: 367–380.

Yang, Q. Q., K. L. Wang, C. H. Zhang, Y. M. Yue, and R. C. Tian. 2011. "Spatio-Temporal of Rocky Desertification and Its Driving Forces in Karst Areas of Northwestern Guangxi, China." *Environmental Earth Sciences* 64: 383–393.

Younis, M. T., M. A. Gilabert, J. Melia, and J. Bastidal. 1997. "Weathering Process Effects on Spectral Reflectance of Rocks in a Semi-Arid Environment." *International Journal of Remote Sensing* 18: 3361–3377.

Yuan, D. X., and C. Zhang. 2008. "Karst Dynamics Theory in China and Its Practice." *Geoscience Sina* 29: 355–365.

Yue, Y. M., K. L. Wang, B. Zhang, B. Liu, H. S. Chen, and M. Y. Zhang. 2011. "Uncertainty of Remotely Sensed Extraction of Information of Karst Rocky Desertification." *Advance in Earth Sciences* 26: 266–274.

Yue, Y. M., B. Zhang, K. L. Wang, B. Liu, R. Li, H. S. Chen, M. Y. Zhang, and Q. Q. Yang. 2010. "Spectral Indices for Estimating Ecological Indicators of Karst Rocky Desertification." *International Journal of Remote Sensing* 31: 2115–2122.

Zhang, P. P., Y. M. Hu, and D. N. Xiao. 2010. "A Method of the Percentage of Bare Rock Calculation in Karst Areas Based on Multispectrum Remote Sensing Image." *Remote Sensing Technology Applications* 25: 510–514.

Zhou, Q., M. Robson, and P. Pilesjo. 1998. "On the Ground Estimation of Vegetation Cover in Australian Rangelands." *International Journal of Remote Sensing* 9: 1815–1820.